Received: 30 August 2024 | Revised: 1 November 2024 | Accepted: 22 November 2024

DOI: 10.1002/alz.14475

Alzheimer's & Dementia®
THE JOURNAL OF THE ALZHEIMER'S ASSOCIATION

RESEARCH ARTICLE

Neural deterioration and compensation in visual short-term memory among individuals with amnestic mild cognitive impairment

Ye Xie[1,2] | Tinghao Zhao[1] | Wei Zhang[3,4] | Qi Chen[2] | Anqi Qiu[5] | Yunxia Li[3,4,6] | Yixuan Ku[1,7]

[1]Guangdong Provincial Key Laboratory of Brain Function and Disease, Center for Brain and Mental Well-Being, Department of Psychology, Sun Yat-sen University, Guangzhou, China

[2]School of Psychology, Shenzhen University, Shenzhen, China

[3]Department of Neurology, Shanghai Pudong Hospital, Fudan University Pudong Medical Center, Pudong, Shanghai, China

[4]Department of Neurology, Tongji Hospital, School of Medicine, Tongji University, Shanghai, China

[5]Department of Health Technology and Informatics, Hong Kong Polytechnic University, Hong Kong, China

[6]Shanghai Key Laboratory of Vascular Lesions Regulation and Remodeling, Pudong, Shanghai, China

[7]Peng Cheng Laboratory, Shenzhen, China

Correspondence
Yixuan Ku, Guangdong Provincial Key Laboratory of Brain Function and Disease, Center for Brain and Mental Well-Being, Department of Psychology, Sun Yat-sen University, Guangzhou 510006, China.
Email: kuyixuan@mail.sysu.edu.cn

Yunxia Li, Department of Neurology, Shanghai Pudong Hospital, Fudan University Pudong Medical Center, 2800 Gongwei Road, Pudong, Shanghai 201399, China.
Email: doctorliyunxia@163.com

Funding information
National Natural Science Foundation of China, Grant/Award Number: 32171082 32471136; National Social Science Foundation of China, Grant/Award Number: 17ZDA323; Neuroeconomics Laboratory of Guangzhou Huashang College, Grant/Award Number: 2021WSYS002; the Science and Technology Planning Project of Guangdong Province, Grant/Award Number: 2023B1212060018; Database Project of Tongji Hospital of Tongji University, Grant/Award Number: TJ(DB)2102; Clinical Research Project of

Abstract

INTRODUCTION: Visual short-term memory (VSTM) is a critical indicator of Alzheimer's disease (AD), but whether its neural substrates could adapt to early disease progression and contribute to cognitive resilience in amnestic mild cognitive impairment (aMCI) has been unclear.

METHODS: Fifty-five aMCI patients and 68 normal controls (NC) performed a change-detection task and underwent multimodal neuroimaging scanning.

RESULTS: Among the atrophic brain regions in aMCI, VSTM performance correlated with the volume of the right prefrontal cortex (PFC) but not the medial temporal lobe (MTL), and this correlation was mainly present in patients with greater MTL atrophy. Furthermore, VSTM was primarily correlated with frontal structural connectivity in aMCI but was correlated with more distributed frontal and MTL connectivity in NC.

DISCUSSION: This study provided evidence on neural adaptation in the precursor stages of AD, highlighting the compensatory role of PFC as MTL deteriorated and suggesting potential targets in early intervention for cognitive preservation.

KEYWORDS
Alzheimer's disease, amnestic mild cognitive impairment, cognitive resilience, medial temporal lobe, prefrontal compensation, prefrontal cortex, visual short-term memory

Ye Xie and Tinghao Zhao are co-first authors and contributed equally to this study.

Tongji Hospital of Tongji University, Grant/Award Number: ITJ(ZD)2002; Shanghai Hospital Development Center Foundation, Grant/Award Number: SHDC12021110; Shanghai Committee of Science and Technology, Grant/Award Number: 22Y11903500; Guangdong Basic and Applied Basic Research Foundation, Grant/Award Number: 2022A1515110105; Fundamental Scientific Research Business Expense for Higher School of Central Government, Grant/Award Number: 22qntd6403; Project funding from Shanghai Municipal Health Commission, Grant/Award Number: 2022JC018; Science and Technology Development Fund of Shanghai Pudong New Area, Grant/Award Number: PKJ2024-Y53; the Leading Talent Program at Sun Yat-sen University, Grant/Award Number: 31620016

Highlights

- Atrophic left medial temporal lobe (MTL) no longer correlated with visual short-term memory (VSTM) in amnestic mild cognitive impairment (aMCI).
- Atrophic right middle frontal area continued to correlate with VSTM in aMCI.
- Frontal brain–behavior correlation was mainly present in the aMCI subgroup with greater medial temporal lobe (MTL) atrophy.
- Reliance of VSTM on frontal connectivity increased in compensation for MTL dysfunction.

1 | BACKGROUND

Amnestic mild cognitive impairment (aMCI) is a prodromal state of Alzheimer's disease (AD) with memory loss as the predominant symptom.[1,2] While a substantial number of individuals with aMCI progress rapidly to AD, variability exists in which some manage to maintain their cognitive functions for a relatively extended period.[3,4] This variation raises important questions: what is the impact of disease pathology on the neural correlates of cognitive function? Could the neural correlates adapt in response to pathology and contribute to prolonged cognitive stability? Addressing these questions may help us understand the neurocognitive changes along the progression of the disease and develop strategies for preserving cognitive function at the early stages of the disease and delaying the conversion to AD.[5]

One cognitive domain of particular interest is visual short-term memory (VSTM), which is crucial yet vulnerable to AD pathology. VSTM typically involves a binding process in which visual features are integrated into unified representations to form item identities for temporary maintenance in memory, providing the basis for further manipulation and complex thinking.[6,7] Recently, VSTM has been flagged as a highly sensitive behavioral marker of disease progression across the AD spectrum and was found to be compromised even among asymptomatic carriers of familial AD who performed normally on conventional neuropsychological tests.[8–10] VSTM performance has also been linked to tau and amyloid beta burdens in carriers of familial AD[11] and could effectively discriminate mild cognitive impairment (MCI) from healthy controls at a very early stage of cognitive decline.[12] These findings revealed a close relationship between VSTM decline and AD progression. However, whether the corresponding neural substrates would reorganize along the procedure of pathology has been largely uninvestigated.

Previous research has identified the prefrontal cortex (PFC) as the primary neural substrate supporting VSTM[13,14] and also placed increasing emphasis on the hippocampus and the medial temporal lobe (MTL).[15,16] PFC has been associated with top-down control in maintaining task-relevant information and filtering out irrelevant distractions.[15,17] The hippocampus has been associated with the performance of VSTM binding and precision.[18–20] Both PFC and MTL exhibited persistent neuronal activity during VSTM processing[14,21] and the cross-frequency phase-amplitude coupling between these two areas has been suggested to be critical for successful mnemonic processing.[22,23] In AD pathology, the MTL is known to be particularly vulnerable as brain atrophy has been proposed to progress from limbic and medial temporal areas to higher-order association areas.[24,25] Interestingly, previous studies have reported increased activity in the frontoparietal area during VSTM processing in individuals with MCI compared to normal controls (NCs) and those with AD.[26,27] This suggested that the neural substrate of short-term memory may change to emphasize prefrontal function when cortical atrophy most prominently affects MTL function at the early stages of the disease, potentially representing a neuroadaptive mechanism that supports cognitive resilience among MCI individuals. However, it remains unclear whether the altered neural correlates are specific to short-term memory processing as the verbal nature of the task material could introduce susceptibility to semantic interference.[28] In contrast, VSTM primarily engages visual information processing and is less susceptible to semantic and verbal strategies, making it a better tool to detect the impairment in short-term memory per se.[29]

The current study aimed to shed light on the neural mechanism behind cognitive resilience in VSTM under the effects of early AD pathology. We hypothesized that neural deterioration, particularly atrophy of the MTL, would lead to dysfunction of the original neural substrate of VSTM, while neural adaptation, such as compensation from the PFC, would help sustain cognitive functions. By examining the relations between VSTM performance and multimodal neuroimaging measures, the current study revealed significant reorganization of the neural correlates underlying VSTM function in the face of disease progression in aMCI.

2 | METHODS

2.1 | Diagnostic assessment

The diagnosis of aMCI was carried out by neurologists from Tongji Hospital, Shanghai in accordance with the MCI criteria for the clinical and cognitive syndrome from the National Institute on Aging–Alzheimer's Association.[30] Specifically, the criteria included: (a) the participant and the caregiver had complaints of memory/cognitive decline; (b) Mini-Mental State Examination (MMSE) or Montreal Cognitive Assessment (MoCA) scores met criteria adjusted by education; (c) Clinical Dementia Rating (CDR) Scale of 0.5; (d) participants met at least one of the following three criteria: (1) performance in at least two cognitive domains fell below the established cutoff (> 1 standard deviation [SD]); (2) at least two cognitive domains were impaired (> 1 SD); (3) functional limitations in more than one area of Instrumental Activities of Daily Living (IADL-14), with a score of ≥ 1. These criteria allowed for the accurate identification of an aMCI cohort that represented the transitional stage between normal aging and AD and ensured the clinical significance and reliability of our findings.

RESEARCH IN CONTEXT

1. **Systematic review**: A PubMed search found that studies show visual short-term memory (VSTM) is affected by Alzheimer's disease (AD), possibly serving as an early sign of the condition. Yet, there's a lack of research comparing how VSTM relates to brain function in those with mild cognitive issues or AD versus healthy people, especially regarding how the brain adapts as the disease advances.
2. **Interpretation**: This study offers insights into how the brain adapts to support VSTM in the early phases of AD. It lays the groundwork for understanding cognitive resilience in amnestic mild cognitive impairment (aMCI), helping to explain the brain's response to early cognitive decline.
3. **Future directions**: Future studies should use long-term research and brain imaging to better understand how the brain adapts and its link to cognitive resilience. This could lead to new ways to detect and treat AD early on.

2.2 | Participants

A total of 123 participants were recruited from Tongji Hospital. The participants included 55 individuals diagnosed with aMCI and 68 age-matched NCs ranging from 60 to 90 years old. The two groups were matched in age but differed in education level and sex ratio (see Table 1 for a summary of demographic statistics), which were regressed out as covariates in subsequent analyses. Significant differences in MMSE and MoCA scores were observed between the two groups. The study was approved by the institutional review board at Tongji Hospital and informed consent was obtained from all participants.

2.3 | Behavioral data analyses

VSTM function was assessed using a modified color change detection task (Figure 1A).[31,32] A fixation cross was presented in the center of the screen throughout the task. An arrow first appeared on the top of the screen for 200 ms as a cue of to which hemifield the participants should attend. After another 300 ms, a memory array was presented for 500 ms and the participants remembered the items on the hemifield indicated by the arrow. The array consisted of two or four colored squares on each side of the fixation cross. After a 900 ms delay period, a test array was presented and the participants pressed correspondent buttons to indicate whether the test array was identical to the memory array. The test array was presented until a response was given.

Response accuracy and mean reaction time (RT) were calculated for each participant under each memory load condition. Memory capacity was estimated based on the performance in the 4-item condition using Cowan's K coefficient (calculated by "load × [hit rate – false alarm rate]").[33] Repeated measure analysis of variance (ANOVA) was used to test for between-group differences in accuracy and RT and analysis of

TABLE 1 demographic characteristics.

	aMCI ($n = 55$)	NC ($n = 68$)	Between-group differences
Age (years)	72.42 (6.69)	70.31 (6.19)	$t(121) = 1.81, p = 0.072$[a]
Sex (male:female)	23:32	44:24	$\chi^2 = 6.42, p = 0.011$[b]
Education (years)	11.33 (2.65)	12.43 (2.79)	$t(121) = -2.22, p = 0.028$[a]
MMSE	24.86 (2.48)	27.47 (1.65)	$W = 638.5, p < 0.001$[c]
MoCA	17.07 (3.34)	24.24 (2.48)	$t(121) = -13.64, p < 0.001$[a]

Note: Values = mean (standard deviation).
Abbreviations: aMCI, amnestic mild cognitive impairment; MMSE, Mini-Mental State Examination; MoCA, Montreal Cognitive Assessment; NC, normal control.
[a]Independent two-sample *t* test.
[b]Chi-square test.
[c]Mann–Whitney *U* test.

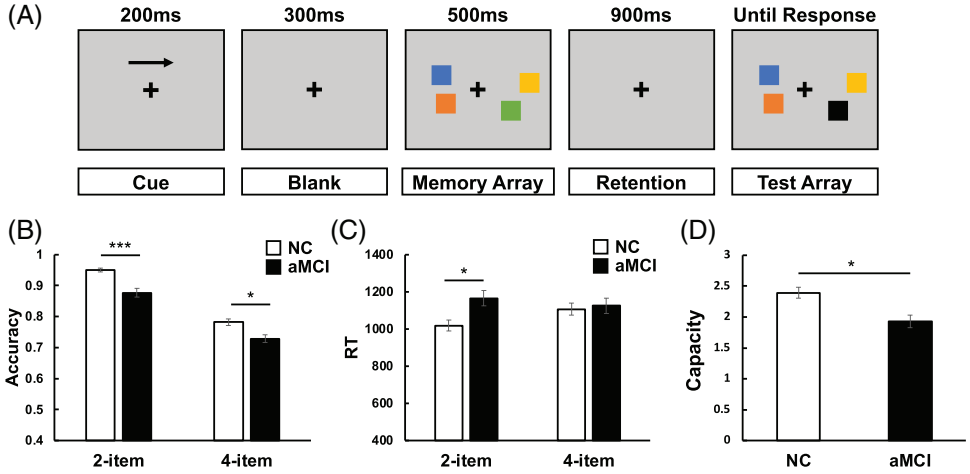

FIGURE 1 A, Stimuli and trial procedure of visual change detection task. B–D, Performance of change detection task. Error bar represents standard error. Age, sex, education, and collection site were used as covariates. $^{*}p < 0.05$; $^{**}p < 0.005$; $^{***}p < 0.001$. aMCI, amnestic mild cognitive impairment; NC, normal control; RT, reaction time.

covariance (ANCOVA) was used to test for between-group differences in memory capacity. The significance threshold was set at $p < 0.05$ after Bonferroni correction and age, sex, education, and the collection site of imaging data (see below) were used as covariates.

2.4 | Magnetic resonance imaging acquisition

Imaging data were collected from Tongji Hospital using a Siemens Verio machine and a 32-channel head coil (20 aMCI participants and 27 NC participants) and from East China Normal University using a Siemens Prisma machine and a 64-channel head coil (35 aMCI participants and 41 NC participants). There was no significant between-group difference in the distribution of the collection site ($\chi^2 = 0.144$, $p = 0.704$). To control for the difference in equipment and scanning parameters, collection site was used as a covariate in all analyses involving the imaging data.

At Tongji Hospital, T1-weighted structural imaging was acquired with echo time (TE) = 2.98 ms, repetition time (TR) = 2530 ms, field of view (FOV) = 256 mm × 256 mm, acquisition matrix = 256 × 256, and reconstruction voxel size = 0.5 × 0.5 × 1.0 mm^3. Resting-state functional imaging was acquired with TR = 500 ms, TE = 30 ms, FOV = 224 mm × 224 mm, matrix = 64 × 64, 25 interleaved slices, and a total of 960 scans. For 27 participants (10 aMCI participants, 17 NC participants), high angular resolution diffusion-weighted images were acquired with 64 gradient directions, $b = 1000$ s/mm^2, TR = 13700 ms, TE = 85 ms, 75 transverse slices, voxel size = 2 × 2 × 2 mm. For 20 participants (10 aMCI participants, 10 NC participants), diffusion kurtosis images were acquired with 30 directions of $b = 1000$ s/mm^2, 30 directions of $b = 2000$ s/mm^2, TR = 8500 ms, TE = 98 ms, 40 transverse slices, and voxel size = 3 × 3 × 3 mm^3. Directions with $b = 2000$s/mm^2 were removed prior to analysis for consistency across participants.

At East China Normal University, T1-weighted structural imaging was acquired with TE = 2.98 ms, TR = 2530 ms, FOV = 256 mm × 256 mm, acquisition matrix = 256 × 256, and reconstruction voxel size = 1.0 × 1.0 × 1.0 mm^3. Resting-state functional imaging was acquired with TR = 2000 ms, TE = 30 ms, FOV = 224 mm × 224 mm, matrix = 64 × 64, 31 interleaved slices, and a total of 240 scans. High angular resolution diffusion-weighted images were acquired with 64 gradient directions of $b = 1000$ s/mm^2, 64 directions of $b = 2000$ s/mm^2, TR = 2400 ms, TE = 71 ms, 76 transverse slices, and voxel size = 2 × 2 × 2 mm^3 for 76 participants (35 aMCI participants, 41 NC participants). Directions with $b = 2000$ s/mm^2 were removed prior to analysis for consistency.

2.5 | Voxel-based morphometry analysis

To examine the gray matter structural integrity of aMCI and normal individuals, we extracted whole-brain volumes using a voxel-based morphometry (VBM) method. T1-weighted images were manually aligned to conventional anterior commissure (AC) – posterior commissure (PC) space with AC, PC, and the midsagittal plane as landmarks and were analyzed with CAT toolbox (http://www.neuro.uni-jena.de/cat/) implemented in Statistical Parametric Mapping (SPM12) software (https://www.fil.ion.ucl.ac.uk/spm/software/spm12/). The preprocessing procedure included skull stripping, segmentation into gray matter, white matter, and cerebrospinal fluid probability images, and spatial normalization of the gray matter images to a customized gray matter template in standard Montreal Neurological Institute (MNI) space. Gray matter probability maps were held at the threshold of 0.1 to minimize the inclusion of incorrect tissue types. The images were modulated with Jacobian determinants and were smoothed with an isotropic Gaussian kernel (8 mm full-width half maximum [FWHM]) after segmentation.

A two-sample *t* test was performed to test the between-group difference in gray matter volume with total intracranial volume (TIV), age, sex, education, and collection site as covariates. A voxel-wise thresh-

old of $p < 0.005$ and a cluster-level threshold of $p < 0.05$ was applied using the Gaussian random field (GRF) theory method provided in DPABI toolbox.[34] Significant clusters were identified after applying an AAL (anatomical automatic labeling) mask of 90 gray matter regions.[35] Anatomical labels of the clusters were determined using the AAL,[35] the Harvard–Oxford atlas,[36] and the Juelich histological atlas.[37] Follow-up Pearson correlation analysis examined the relationship between the region of interest (ROI; i.e., clusters identified from whole-brain analysis) volumes and VSTM performance with TIV, age, sex, education, and collection site as covariates.

2.6 | Functional magnetic resonance imaging data preprocessing and connectivity analysis

Functional images from the first 10 seconds were discarded for signal equilibrium before preprocessing and analysis using the CONN toolbox.[38] The preprocessing procedure included realignment and unwrapping, slice timing correction, segmentation and normalization, and Gaussian kernel smoothing (8 mm FWHM). Nine participants in the aMCI group and four participants in the NC group were excluded due to excessive head motion (displacement > 3 mm or rotation > 3°) and the remaining 46 aMCI participants and 64 NC participants were included in the following analysis. In addition to the six motion parameters and their first derivatives, white matter signals and cerebrospinal fluid signals were removed using the CompCor method.[39] This component-based noise correction method reduces physiological and extraneous noise and provides interpretative information on correlated and anticorrelated functional brain networks. Detrending and a 0.008 to 0.08 Hz band-pass filter were also applied for further noise reduction.

For analyses of the functional data, we focused on the atrophic brain regions that showed association with VSTM in the VBM analysis. These areas were used as seed regions of interest (ROI seeds) and seed-to-voxel functional connectivity was assessed within the rest of the brain. A two-sample *t* test was then performed to identify between-group differences in functional connectivity with age, sex, education, and collection site as covariates. A voxel-wise threshold of $p < 0.005$ and a cluster-level threshold of $p < 0.05$ was applied using the GRF method provided in DPABI toolbox.[34] Significant clusters were determined after applying a gray matter mask of AAL 90 regions.[35] Anatomical labels of the clusters were determined using the AAL,[35] the Harvard–Oxford atlas, and the Juelich histological atlas. Follow-up Pearson correlation analysis examined the relationship between VSTM performance and between-group differences in functional connectivity with age, sex, education, and collection site as covariates.

2.7 | Median-split analysis

In each of the aMCI and NC groups, participants were median split into a subgroup with a larger volume (LV) of left MTL and a subgroup with a smaller volume (SV) of left MTL to examine the impact of disease progression on the relationship between VSTM performance and the atrophic right middle frontal gyrus (MFG) as found in the VBM analysis. The brain–behavioral association was then calculated in each subgroup for brain areas showing a significant correlation with VSTM performance in the whole group, with age, sex, education, TIV, and collection site as covariates.

2.8 | Native-space T1-weighted image segmentation

Prior to constructing whole-brain connectomes from the diffusion-weighted imaging (DWI) data, a 91-region segmentation was first created based on the structural imaging data. T1-weighted (T1-w) images were processed in FreeSurfer v7 (https://surfer.nmr.mgh.harvard.edu/) using the "recon-all" command with default parameters. All images were reconstructed into 256 x 256 x 256 resolution with 1-mm isotropic voxels and whole-brain segmentation was performed based on the "aparc+aseg" template. In particular, the segmentation divided MTL into the anterior/posterior hippocampus, entorhinal cortex, and parahippocampal cortex. Because the MTL was a key ROI to our study, we further performed a more accurate segmentation of the MTL based on the ASHS-PMC-T1 atlas[40] using the Automatic Segmentation of Hippocampal Subfields (ASHS) tool,[41] which additionally included two perirhinal cortex segments (Brodmann area 35 and 36).

In generating a final segmentation for connectome construction, MTL segments from the FreeSurfer segmentation were first removed using the fslmaths function from FSL.[43] An inversed mask of all MTL segments from ASHS (except for Brodmann area 36) was then applied to the MTL-removed FreeSurfer segmentation using the mri_mask function from FreeSurfer. All MTL segments from ASHS were added to the processed segmentation except for Brodmann area 36, which overlapped with the fusiform gyrus from the FreeSurfer segmentation. In addition, as white matter areas in the MTL are usually thin and may get misassigned to gray matter areas in automatic segmentation, the white matter segment was dilated by a sphere of 1-mm radius to prevent the white matter pathways from being obstructed during automatically constrained fiber tracking.

In addition, hippocampal atrophy in MCI patients may result in enlarged hippocampal fissure, which is not taken into account in the segmentations described above. To acquire a more accurate estimation of hippocampal gray matter volume that excludes the hippocampal fissure, we further performed a hippocampal subfield segmentation using the segmentHA_T1 algorithm provided in FreeSurfer v7,[42] which further divided the hippocampus into the following subfields: parasubiculum, pre-subiculum, subiculum, CA1, CA3, CA4, hippocampus molecular layer, granule cell and molecular layers of the dentate cortex (GC-ML-DC), hippocampus-amygdala transition area (HATA), fimbria, hippocampal tail, and hippocampal fissure. Volumes of the left/right whole hippocampus head and body were estimated by the algorithm based on this segmentation (excluding the hippocampal tail and hippocampal fissure) and were used to replace the estimations generated by ASHS for left/right anterior and posterior hippocampus in the subsequent volume CCA analyses.

2.9 | DWI data processing

A whole-brain white matter connectome was constructed with the probabilistic tractography method. An Eddy current correction was first performed on the raw DWI images in FSL before further processing in MRtrix3.[44] A response function was estimated based on the DWI images using the dwi2response function. Voxel-wise fiber orientation distributions were estimated using the dwi2fod function with constrained spherical deconvolution based on the response function. Ten million streamlines were generated using anatomically constrained probabilistic tractography (tckgen -act, algorithm = iFOD2, dynamic seeding, backtracking allowed, streamline endpoints cropped at gray matter–white matter interface) with anatomical boundaries based on a five-tissue-type segmentation image generated from a skull-stripped T1-w image. A 4560 × 4560 structural connectome was then generated by assigning each streamline to regions in the modified segmentations described earlier using the tck2connectome function.

Instead of directly using the number of streamlines connecting two regions as a measure of connection density, we followed a practice of intersubject normalization[45,46] to allow for proper comparisons of connection density between subjects and groups. First, spherical deconvolution informed filtering of tractograms 2 (SIFT-2)[47] was performed, which generated a weighting factor for each streamline that adjusts its density to be proportional to the underlying white matter fiber density, resulting in a value of apparent fiber density (AFD) that quantifies the relative cross-sectional area of the white matter fibers connecting two brain regions. The ratios of a subject's response function size to the group average response function size at each *b* value were calculated and their geometric mean was multiplied with the connectome constructed from the AFD values of all streamlines. To account for individual differences in white matter *b*0 intensity, the ratio of the mean median *b*0 value within the subject's white matter mask to the grand mean median *b*0 value of the group was calculated and multiplied with the connectome. Finally, individual differences in connection density were accounted for by scalar multiplying the connectome by the proportionality coefficient μ derived from SIFT-2, which represents the estimated fiber volume per unit length contributed by each streamline.

After acquiring the normalized connectome for all subjects, we removed connections that had zero values in all subjects and connections that connected contra-lateral regions. Consistency-based thresholding[48] was then performed to filter connections by their group consistency instead of average density, so that structural connections that are weak but consistently present within the group would not be discarded. Connections were ranked by the coefficient of variation (= SD/mean) and thresholded at the 75th percentile. A total of 1408 connections remained after the screening.

2.10 | Canonical correlation analysis

We used canonical correlation analysis (CCA) to identify the joint relationship between structural connections/gray matter volumes and VSTM performance measures, including two-item and four-item accuracy and memory capacity. CCA is a powerful multivariate tool that calculates the correlation between two sets of variables by identifying two linear combinations of the variables that are maximally correlated.[49,50] The full procedure of the analysis (see Figure S1 in supporting information) was implemented in R and CCA was conducted using the rcc function from the mixOmics package.[51] Prior to all analyses, the linear effects of age, education, sex and collection site on all behavioral and neural measures were regressed out. Additionally, TIV was regressed out from all neural measures and the method of DWI scanning was regressed out from all structural connection measures.

A feature selection procedure[52] was first performed to rank the connections by how robustly they are correlated with a target measure. In each of the 1000 replicates, we subsampled 90% of the full data and calculated the Pearson correlation between each connection/volume (***X*** variable) and each WM measure (***Y*** variable). The ***X*** variables were ranked by their average correlation *p* values across all subsamples. The canonical correlations between the ***Y*** variables and the top *n* ***X*** variables in the rank list were then calculated for the range $n = 5$ to 50 by bins of 5. For each canonical correlation, the loadings of the ***X*** variables were calculated and the significance threshold was set at $P < 0.001$, false discovery rate corrected. The canonical correlation that generated the greatest number of significant ***X*** variable loadings was selected as the final result of the analysis. In the structrual connection analysis, we restricted the X variables to all available connections with frontal and medial temporal regions (see supporting information for lists of region labels).

3 | RESULTS

3.1 | Change detection task performance

Two-way repeated measures ANOVA revealed a significant main effect of group in accuracy ($F[1,117] = 15.38$, $p < 0.001$, partial $\eta^2 = 0.116$; Figure 1B) and the post hoc *t* tests revealed significantly lower accuracy of both two-item ($p < 0.001$) and four-item ($p = 0.049$) change detection task in the aMCI group than in the NC group (Bonferroni corrected). There is a significant main effect of group ($F[1,117] = 5.26$, $p = 0.024$, partial $\eta^2 = 0.043$) and a significant interaction between group and load ($F[1,117] = 8.62$, $p = 0.004$, partial $\eta^2 = 0.069$) in RT (Figure 1C). Post hoc *t* tests showed significantly longer RT of two-item ($p = 0.011$) change detection task in the aMCI group than in the NC group in (Bonferroni corrected). ANCOVA also showed significantly lower memory capacity in the aMCI group compared to the NC group ($F[1,117] = 8.382$, $p = 0.005$, partial $\eta^2 = 0.067$; Figure 1D). Together, these results agreed with previous findings of VSTM deficits in aMCI population.

3.2 | Brain–VSTM correlation under cortical deterioration

We first examined the gray matter structural integrity of aMCI participants and its association with VSTM performance. A two-sample *t*

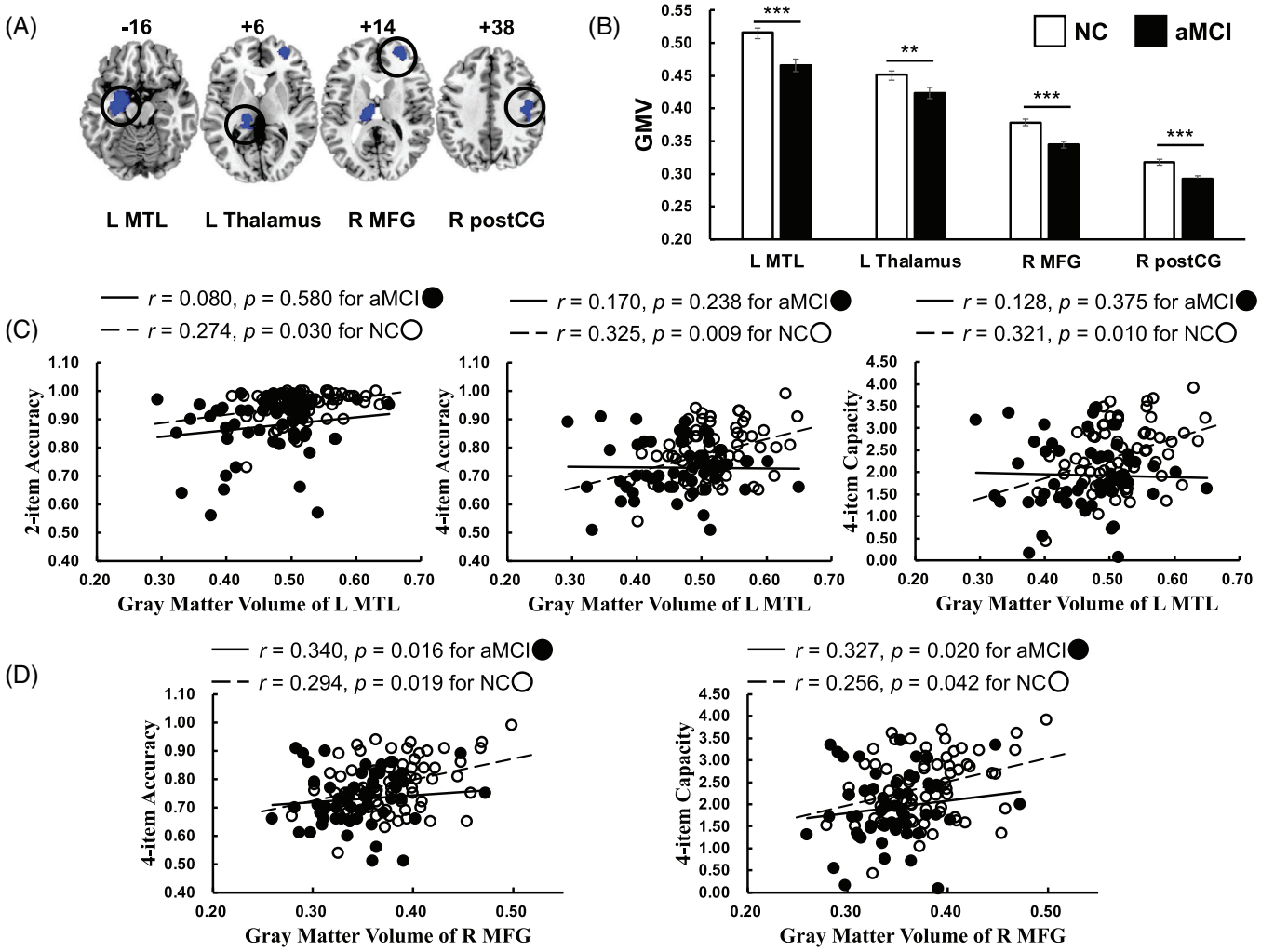

FIGURE 2 A, Structural atrophy in aMCI group compared to NC group. Voxel-wise threshold $p < 0.005$, cluster-level threshold $p < 0.05$ with GRF correction, gray matter mask applied. B, Significant structural differences between NC and aMCI group. Error bar represents standard error. $^{**}p < 0.005$; $^{***}p < 0.001$. C, Relationship between structural GMV of left MTL and performance of change detection task for each group. D, Relationship between structural GMV of right MFG and performance of change detection task for each group. Age, sex, education, TIV, and collecting site were used as covariates for the analysis above. aMCI, amnestic mild cognitive impairment; GRF, Gaussian random field; GMV, gray matter volume; HP, hippocampus; L, left; MFG, middle frontal gyrus; MTL, medial temporal lobe; NC, normal control; postCG, postcentral gyrus; R, right; TIV, total intracranial volume.

test showed that the volumes of left thalamus (peak coordinate: −18, −33, 6), right postcentral gyrus (postCG; peak coordinate: 44, −18, 38), left MTL (including hippocampus/amygdala area; peak coordinate: −27, −10, −16) and right MFG (peak coordinate: 24, 54, 14) were significantly smaller in the aMCI group compared to the NC group (Figure 2A,B and Table S1 in supporting information, voxel-wise threshold $p < 0.005$, cluster-level threshold $P < 0.05$ by GRF correction). Further correlation analyses showed that the volume of left MTL was positively correlated with accuracy in both two-item and four-item conditions and with memory capacity of the change detection tasks in the NC group but not in the aMCI group (*ps* > 0.05; Figure 2C). The volume of right MFG was positively correlated with accuracy in the four-item condition and memory capacity in both the aMCI group and the NC group (Figure 2D). No significant correlation was found between the VSTM performance and the volume of left thalamus or right postCG.

Next, we used the left MTL cluster and the right MFG cluster described above as seed regions and tested for between-group difference in functional connectivity and their correlation with change detection task performance. Seed to whole-brain analysis showed significantly greater connectivity between the left MTL seed and right superior frontal gyrus/middle frontal gyrus (SFG/MFG; peak coordinate: 16, 46, 26) in the aMCI group compared to NC group while no significant difference was found for connectivity with the right MFG seed (Figure 3A,B and Table S2 in supporting information, voxel-wise threshold $p < 0.005$, cluster-level threshold $P < 0.05$ by GRF correction). This identified area was adjacent to the right MFG area that showed significant atrophy in the aMCI group (Figure 3C). However, further

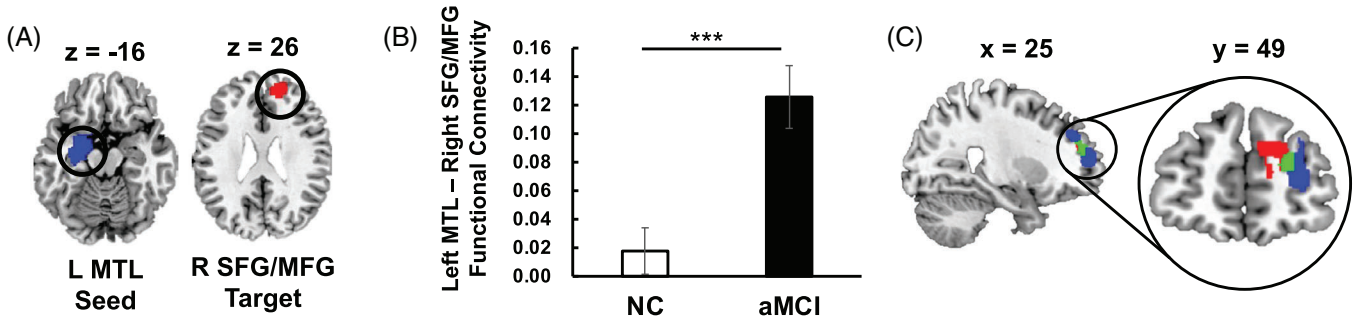

FIGURE 3 A, Right SFG/MFG (target) area showed significant between-group difference in functional connectivity to left MTL (ROI seed). Voxel-wise threshold $p < 0.005$, cluster-wise threshold $p < 0.05$ with GRF correction, gray matter mask applied and age, sex, education, and collecting site as covariates. B, Significant between-group difference in functional connectivity between left MTL and right SFG/MFG. Error bar represents standard error; $^{***}p < 0.001$. C, Display of the right frontal areas. Red, the right SFG/MFG in functional results; blue, the right MFG in structural results; green, overlap area. aMCI, amnestic mild cognitive impairment; GRF, Gaussian random field; MCI, mild cognitive impairment; L, left; MFG, middle frontal gyrus; MTL, medial temporal lobe; NC, normal control; R, right; ROI, region of interest; SFG, superior frontal gyrus.

correlation analyses revealed no significant correlation between the identified connectivity and VSTM performance in either group.

3.3 | The impact of disease progression on brain-VSTM association in PFC

Given that significant correlation between right MFG volume and VSTM performance was found in both groups, it remains unclear whether this association reflects a preservation of the original frontal substrate or an altered neural substrate that emerged in response to worsened MTL atrophy. We median-split the aMCI participants into two subgroups by the volumes of the atrophic left MTL area and examined the impact of disease progression, characterized by the severity of left MTL atrophy here, on the relationship between VSTM performance and the atrophic right MFG. No significant difference in VSTM performance or right MFG volumes was found between the subgroups except RT, in which the RT was longer in the subgroup with a SV of left MTL compared to the subgroup with a LV of left MTL (Table S3 in supporting information). Importantly, a significant positive correlation between VSTM performance and right MFG volume was found in the SV subgroup but not in the LV subgroup (Figure 4), suggesting that this correlation was not a continuous preservation of the original frontal correlation but may represent a new neural substrate that emerged as MTL atrophy worsened.

3.4 | Reorganized VSTM neural substrate in aMCI

To further investigate the new substrate underlying VSTM in aMCI, we calculated white matter structural connectivity constructed from DWI data and computed correlations with VSTM performance using CCA. The results showed that VSTM performance was correlated with a variety of connections in the NC group, including frontal–parietal, frontal–frontal, MTL–visual, and MTL–subcortical connections (Figure 5A and Table S4 in supporting information). On the other hand, VSTM performance was mainly correlated with frontal–parietal and frontal–MTL connections in the aMCI group (Figure 5B and Table 2). This pattern is consistent with the findings that VSTM was correlated with right MFG volume in both groups but correlated with left MTL volume only in the NC group. In addition, the significant VSTM correlation with frontal–MTL connections in the aMCI group also coincides with the higher right SFG/MFG–left MTL functional connectivity we found.

Finally, we also used CCA to test the correlations between VSTM performance and whole-brain segmented gray matter volumes. Again, consistent with earlier findings of VBM-based analysis, CCA revealed that VSTM performance was correlated with the volumes of MTL, prefrontal, and parietal regions in the NC group (Table S5 in supporting information) but was mainly correlated with prefrontal and subcortical regions in the aMCI group (Table 3).

4 | DISCUSSION

In the current study, we investigated the impact of neural deterioration on the neural correlates of VSTM and gathered evidence for the neural reorganization underlying VSTM in the context of early AD, focusing specifically on the aMCI phase. Our findings revealed a shift in the neural substrates of VSTM, showing that VSTM performance became increasingly associated with the gray matter volumes and white matter connectivity of the PFC in the aMCI group when MTL atrophy was severe. These findings enhanced our understanding of neural adaptation in early AD, emphasizing the potential compensatory mechanisms that may emerge as the disease progresses.

First, our findings corroborated previous literature on a number of well-established pathological features. Our behavioral results echoed previous findings of VSTM deficit as an early indicator of AD, underscoring its potential as a marker for preclinical detection.[53] Brain atrophy in aMCI, as revealed by the decreased gray matter volumes of the MTL, thalamus, and frontoparietal regions, were also consistent with the neurodegenerative patterns observed in early AD.[54] The dissociation between VSTM and the atrophic MTL area observed in aMCI

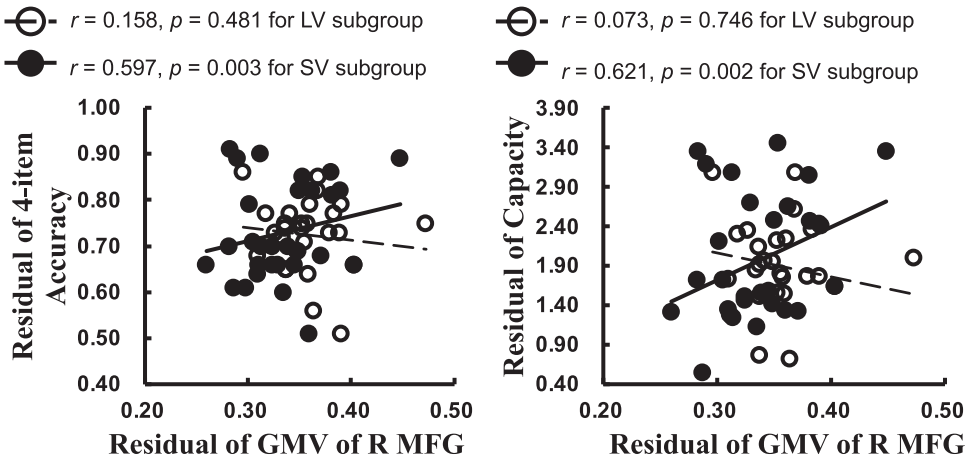

FIGURE 4 Relationship between GMV of right MFG and VSTM performance influenced by the GMV of left MTL in the aMCI group. Age, sex, education, TIV and collecting site were used as covariates. aMCI, amnestic mild cognitive impairment; GMV, gray matter volume; GRF, Gaussian random field; L, left; LV, subgroup with larger volume of left MTL; MFG, middle frontal gyrus; MTL, medial temporal lobe; R, right; SV, subgroup with smaller volume of left MTL.

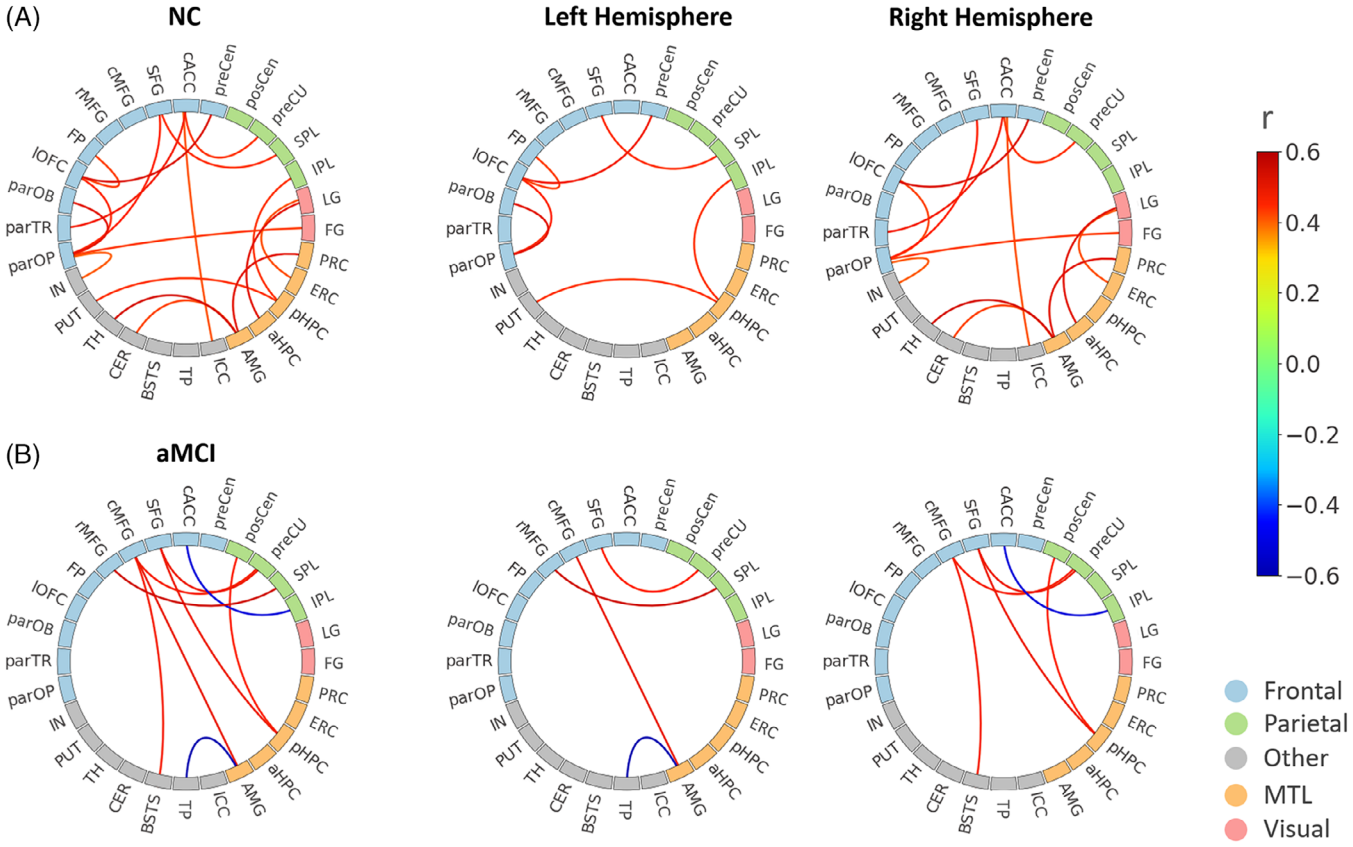

FIGURE 5 Structural connections with significant loadings ($P_{FDR} < 0.001$) in canonical correlation with measures of WM performance (two-item and four-item response accuracies, capacity) for (A) the aMCI group and (B) the NC group, respectively. Line color represents loading correlation coefficient (sign corrected to indicate direction of correlation with WM variables, not the X variate). aHPC, anterior hippocampus; aMCI, amnestic mild cognitive impairment; AMG, amygdala; BSTS, banks of superior temporal sulcus; cACC, caudal anterior cingulate cortex; CER, cerebellum; cMFG: caudal middle frontal gyrus; ERC, entorhinal cortex; FDR, false discovery rate; FG, fusiform gyrus; FP, frontal pole; ICC, isthmus cingulate cortex; IN, insula; IPL, inferior parietal lobe; LG, lingual gyrus; lOFC, lateral orbitofrontal cortex; NC, normal control; parOB, pars orbitalis; parOP, pars opercularis; parTR, pars triangularis; pHPC, posterior hippocampus; posCen, postcentral gyrus; PRC, perirhinal cortex Brodmann area 35; preCen, precentral gyrus; preCU, precuneous; PUT, putamen; rMFG, rostral middle frontal gyrus; SFG, superior frontal gyrus; SPL, superior parietal lobe; TH, thalamus; TP, temporal pole; WM, white matter.

TABLE 2 Canonical correlation analysis results for structural connections and VSTM performance in the aMCI group.

N-feature	*r* (cc)	*p* (cc)
15	0.75	<0.001
***Y* variables**	***r* (load)**	***p* (load)**
Accuracy of 2-item	0.75	<0.001
Accuracy of 4-item	0.92	<0.001
Capacity	0.85	<0.001
***X* variables**	***r* (load)**	***p* (load)**
R.SFG—R.pHPC	0.48	<0.001
L.cMFG—L.AMG	0.49	<0.001
L.rMFG—L.SPL	0.54	<0.001
L.SFG—L.preCU	0.45	<0.001
R.cACC—R.IPL	−0.52	<0.001
R.cMFG—R.preCU	0.46	<0.001
R.cMFG—R.BSTS	0.46	<0.001
R.SFG—R.preCU	0.48	<0.001
L.AMG—L.TP	−0.60	<0.001
R.pHPC—R.posCen	0.45	<0.001

Notes: Canonical correlation (cc) between WM performance and the top N-feature connections for aMCI; loadings (load) of connections (*X* variables) and WM measures (*Y* variables). False discovery rate corrected $P < 0.001$.
Abbreviations: aMCI, amnestic mild cognitive impairment; AMG, amygdala; BSTS, banks of superior temporal sulcus; cACC, caudal anterior cingulate cortex; cMFG, caudal middle frontal gyrus; IPL, inferior parietal lobe; pHPC, posterior hippocampus; posCen, postcentral gyrus; preCU, precuneus; rMFG, rostral middle frontal gyrus; SFG, superior frontal gyrus; SPL, superior parietal lobe; TP, temporal pole; VSTM, visual short-term memory; WM, white matter.

TABLE 3 Canonical correlation analysis results for whole-brain gray matter volume and VSTM performance in the aMCI group.

N-feature	*r* (cc)	*p* (cc)
10	0.52	<0.001
***Y* variables**	***r* (load)**	***p* (load)**
Accuracy of 2-item	−0.88	<0.001
Accuracy of 4-item	−0.81	<0.001
Capacity	−0.81	<0.001
***X* variables**	***r* (load)**	***p* (load)**
L.rMFG	−0.69	<0.001
L.parTR	−0.56	<0.001
L.lOFC	−0.41	0.002
L.mOFC	−0.53	<0.001
L.AC	−0.56	<0.001
R.rMFG	−0.43	<0.001
R.BSTS	−0.63	<0.001
R.AC	−0.56	<0.001
R.TH	−0.67	<0.001
BS	−0.55	<0.001

Notes: Canonical correlation (cc) between WM performance and the top N-feature volumes for aMCI; loadings (load) of volumes (*X* variables) and WM measure (*Y* variables). False discovery rate corrected $P < 0.001$.
Abbreviations: AC, accumbens; aMCI, amnestic mild cognitive impairment; AMG, amygdala; BS, brain stem; BSTS, banks of superior temporal sulcus; lOFC, lateral orbitofrontal cortex; mOFC, medial orbitofrontal cortex; parTR, pars triangularis; rMFG, rostral middle frontal gyrus; TH, thalamus; VSTM, visual short-term memory; WM, white matter.

may have also reflected the impact of neurodegeneration on the role of MTL in VSTM processing as indicated by recent literature.[21]

Although previous literature has highlighted the indicative role of VSTM in AD, the adaptation of the neural correlates of VSTM in response to pathology has rarely been investigated. Adding to the literature, we found a persistent correlation between VSTM and right MFG volume in MCI despite the fact that atrophy was found in this area. Additionally, an adjacent right MFG area exhibited stronger resting-state functional connectivity with the atrophic left MTL. Furthermore, the right MFG–VSTM association was primarily observed in the aMCI subgroup with smaller left MTL volumes. This "re-appeared" association after worsening MTL atrophy might likely represent an adaptive reorganization in which MFG compensated for the deteriorating MTL function rather than a continuous preservation of frontal function throughout the progression of atrophy.[55] In addition, the two subgroups did not differ in response accuracy or memory capacity, suggesting that these compensatory neural correlates may help prevent further decline in VSTM. The frontoparietal network, particularly the MFG, has been proposed to play a critical role in maintaining feature information before episodic memory formation by the hippocampus.[56–58] While previous studies have observed frontal hyperactivities during the maintenance of verbal short-term memory in aMCI,[26,27] the relationship between this hyperactivity and short-term memory performance was not thoroughly examined. By examining the correlation between VSTM and prefrontal area volume at different levels of MTL atrophy, the current study provided distinct evidence for the presence of frontal compensation in the face of severe MTL deterioration.

Further confirming the presence of prefrontal compensation in aMCI, CCA on white matter connectivity revealed a reorganization of the connectivity patterns underlying VSTM in the aMCI group wherein the original dependence on MTL connections found in the NC group diminished and prefrontal connections became the primary neural correlates. Among all the connections with significant loadings, the proportion of the frontal connections was 61% (11/18) in the NC group but increased to 89% (8/9) in the aMCI group. In both groups, VSTM performance was associated with connections between the dorsolateral prefrontal cortex (DLPFC), including the SFG and MFG, and the superior parts of the posterior parietal cortex (PPC), including the superior parietal lobe (SPL) and precuneus. These connections likely reflected neural pathways through the second subdivision of superior longitudinal fasciculus, which is associated with spatial attention and VSTM.[59] In particular, the MFG–SPL pathway has been considered a part of the dorsal stream of visual processing and has been reported to be engaged in VSTM processing.[60] All these findings imply that an

increasing reliance on frontal-parietal pathways for VSTM processing may have developed as the MTL and the pathways connecting it to visual and subcortical regions deteriorated due to brain atrophy or synaptic loss.

Interestingly, we also found a number of frontal–MTL connections correlated with VSTM in the aMCI group. This aligns with our resting state fMRI finding of elevated functional connectivity between the left MTL and the right MFG in aMCI, which may indicate enhanced communication between the MTL and prefrontal system. The PFC and hippocampus are known to communicate through theta oscillation, and their interplay is considered crucial for the encoding, manipulation, and retrieval of working memory,[61–63] as well as for supporting cognitive functions in normal aging.[64] The increased reliance on frontal–MTL connections observed in aMCI may reflect an increased importance of prefrontal control on MTL representation during maintenance.[65] While the precise nature of this finding awaits further investigation, it might suggest that the compensatory mechanism is not a simple replacement of the MTL by the PFC but also entails frontal–hippocampal interactions that complement the reduced capability of the MTL.

Several limitations of this study should be noted. While our findings provided evidence for neural reorganization in aMCI regarding VSTM processing, the cross-sectional nature of the study and the relatively modest sample size did not allow us to draw conclusions on whether this reorganization contributed to the prolonged cognitive stability observed in certain aMCI patients. To answer this question, longitudinal studies with larger sample sizes are needed to closely track the changes in neural substrates over the time course of disease progression. In addition, as our imaging data comprised structural and resting state functional modalities only, evidence from in-task functional data is needed to directly examine the roles of frontal and MTL regions in the VSTM processing of aMCI individuals and provide further insights about the compensation mechanism. Future research can also adapt more complex task designs to probe the source of VSTM error in aMCI subgroups, which would provide further insights into the cognitive processes that were affected as the disease progresses and how these processes were related to the neural reorganization.

In conclusion, the current study advanced our understanding of the neural underpinnings of VSTM under the impact of AD pathology and provided converging evidence of prefrontal compensation as MTL deteriorates in the aMCI phase. These findings laid important groundwork for understanding how cognitive functions may be maintained for extended periods before full-fledged advancement to AD and pointed to the PFC as a potential target for early interventions using non-invasive stimulation techniques like transcranial magnetic stimulation.

AUTHOR CONTRIBUTIONS

Y.K. and Y.L. designed and supervised the study. Y.X., W.Z., and T.Z. conducted the experiment and analyzed the data. Y.X., T.Z., and Y.K. wrote the first draft of the paper. Y.X., T.Z., W.Z., Q.C., A.Q., Y.L., and Y.K. edited the paper.

ACKNOWLEDGMENTS

This work was supported by funding by the National Natural Science Foundation of China (Grant No. 32171082, 32471136), the National Social Science Foundation of China (Grant No. 17ZDA323), the Neuroeconomics Laboratory of Guangzhou Huashang College (2021WSYS002), the Leading Talent Program (31620016) at Sun Yat-sen University, the Science and Technology Planning Project of Guangdong Province (2023B1212060018), the Database Project of Tongji Hospital of Tongji University (Grant No. TJ(DB)2102), Clinical Research Project of Tongji Hospital of Tongji University (Grant No. ITJ(ZD)2002), Shanghai Hospital Development Center Foundation (Grant No. SHDC12021110), Shanghai Committee of Science and Technology, China (Grant No.22Y11903500), Project funding from Shanghai Municipal Health Commission (Grant No.2022JC018), Science and Technology Development Fund of Shanghai Pudong New Area (PKJ2024-Y53), Guangdong Basic and Applied Basic Research Foundation (Grant No. 2022A1515110105), and Fundamental Scientific Research Business Expense for Higher School of Central Government (Grant No. 22qntd6403).

CONFLICT OF INTEREST STATEMENT

The authors declare no conflicts of interest. Author disclosures are available in the supporting information.

DATA AVAILABILITY STATEMENT

Please contact Dr. Yixuan Ku (kuyixuan@mail.sysu.edu.cn) or Dr. Yunxia Li (doctorliyunxia@163.com) if necessary.

CONSENT STATEMENT

The study was approved by the institutional review board at Tongji Hospital and informed consent was obtained from all participants.

ORCID

Yixuan Ku https://orcid.org/0000-0003-2804-5123

REFERENCES

1. Petersen RC, Parisi JE, Dickson DW, et al. Neuropathologic features of amnestic mild cognitive impairment. *Archf Neurol*. 2006;63:665-672. doi:10.1001/archneur.63.5.665
2. Li X, Zhang Z-J. Neuropsychological and neuroimaging characteristics of amnestic mild cognitive impairment subtypes: a selective overview. *CNS Neurosci Ther*. 2015;21:776-783. doi:10.1111/cns.12391
3. Arenaza-Urquijo EM, Vemuri P. Resistance vs resilience to Alzheimer disease: clarifying terminology for preclinical studies. *Neurology*. 2018;90:695-703. doi:10.1212/WNL.0000000000005303
4. Jack CR, Weigand SD, Shiung MM, et al. Atrophy rates accelerate in amnestic mild cognitive impairment. *Neurology*. 2008;70:1740-1752.
5. Yang C, Li X, Zhang J, et al. Early prevention of cognitive impairment in the community population: the Beijing Aging Brain Rejuvenation Initiative. *Alzheimers Dement*. 2021;17:1610-1618. doi:10.1002/alz.12326
6. Wheeler ME, Treisman AM, Binding in short-term visual memory. *J Exp Psychol Gen*. 2002;131:48.
7. Luck SJ, Vogel EK. The capacity of visual working memory for features and conjunctions. *Nature*. 1997;390:279-281. doi:10.1038/36846

8. Kirova AM, Bays RB, Lagalwar S. Working memory and executive function decline across normal aging, mild cognitive impairment, and Alzheimer's disease. *Biomed Res Int*. 2015;2015:748212. doi:10.1155/2015/748212
9. Parra MA, Sala SD, Abrahams S, Logie RH, Méndez LG, Lopera F. Specific deficit of colour–colour short-term memory binding in sporadic and familial Alzheimer's disease. *Neuropsychologia*. 2011;49:1943-1952. doi:10.1016/j.neuropsychologia.2011.03.022
10. Parra MA, Abrahams S, Logie RH, Méndez LG, Lopera F, Della Sala S. Visual short-term memory binding deficits in familial Alzheimer's disease. *Brain*. 2010;133:2702-2713. doi:10.1093/brain/awq148
11. Norton DJ, Parra MA, Sperling RA, et al. Visual short-term memory relates to tau and amyloid burdens in preclinical autosomal dominant Alzheimer's disease. *Alzheimers Res Ther*. 2020;12:99. doi:10.1186/s13195-020-00660-z
12. Parra MA, Calia C, Pattan V, Della Sala S. Memory markers in the continuum of the Alzheimer's clinical syndrome. *Alzheimers Res Ther*. 2022;14:142. doi:10.1186/s13195-022-01082-9
13. Serences JT. Neural mechanisms of information storage in visual short-term memory. *Vis Res*. 2016;128:53-67. doi:10.1016/j.visres.2016.09.010
14. Fuster JM, Alexander GE. Neuron activity related to short-term memory. *Science*. 1971;173:652-654.
15. Rissman J, Gazzaley A, D'Esposito M. Dynamic adjustments in prefrontal, hippocampal, and inferior temporal interactions with increasing visual working memory load. *Cereb Cortex*. 2008;18:1618-1629. doi:10.1093/cercor/bhm195
16. von Allmen DY, Wurmitzer K, Martin E, Klaver P. Neural activity in the hippocampus predicts individual visual short-term memory capacity. *Hippocampus*. 2013;23:606-615. doi:10.1002/hipo.22121
17. Ku Y, Bodner M, Zhou YD. Prefrontal cortex and sensory cortices during working memory: quantity and quality. *Neurosci Bull*. 2015;31:175-182. doi:10.1007/s12264-014-1503-7
18. Olson IR, Page K, Moore KS, Chatterjee A, Verfaellie M. Working memory for conjunctions relies on the medial temporal lobe. *J Neurosci*. 2006;26:4596-4601. doi:10.1523/JNEUROSCI.1923-05.2006
19. Watson PD, Voss JL, Warren DE, Tranel D, Cohen NJ. Spatial reconstruction by patients with hippocampal damage is dominated by relational memory errors. *Hippocampus*. 2013;23:570-580. doi:10.1002/hipo.22115
20. Xie W, Chapeton JI, Bhasin S, et al. The medial temporal lobe supports the quality of visual short-term memory representation. *Nat Hum Behav*. 2023;7:627-641. doi:10.1038/s41562-023-01529-5
21. Liu J, Zhang H, Yu T, et al. Stable maintenance of multiple representational formats in human visual short-term memory. *Proc Natl Acad Sci U S A*. 2020;117:32329-32339. doi:10.1073/pnas.2006752117
22. Wang C, Furlong TM, Stratton PG, et al. Hippocampus–prefrontal coupling regulates recognition memory for novelty discrimination. *J Neurosci*. 2021;41:9617-9632.
23. Brockmann MD, Pöschel B, Cichon N, Hanganu-Opatz IL. Coupled oscillations mediate directed interactions between prefrontal cortex and hippocampus of the neonatal rat. *Neuron*. 2011;71:332-347.
24. Thompson PM, Hayashi KM, Dutton RA, et al. Tracking Alzheimer's disease. *Ann N Y Acad Sci*. 2007;1097:183-214. doi:10.1196/annals.1379.017
25. Whitwell JL, Shiung MM, Przybelski SA, et al. MRI patterns of atrophy associated with progression to AD in amnestic mild cognitive impairment. *Neurology*. 2008;70:512. doi:10.1212/01.wnl.0000280575.77437.a2
26. Bokde ALW, Karmann M, Born C, et al. Altered brain activation during a verbal working memory task in subjects with amnestic mild cognitive impairment. *J Alzheimers Dis*. 2010;21:103-118. doi:10.3233/JAD-2010-091054
27. Maestú F, Yubero R, Moratti S, et al. Brain activity patterns in stable and progressive mild cognitive impairment during working memory as evidenced by magnetoencephalography. *J Clin Neurophysiol*. 2011;28:202-209.
28. Verma M, Howard RJ. Semantic memory and language dysfunction in early Alzheimer's disease: a review. *Int J Geriatr Psychiatry*. 2012;27:1209-1217. doi:10.1002/gps.3766
29. Pavisic IM, Suarez-Gonzalez A, Pertzov Y. Translating visual short-term memory binding tasks to clinical practice: from theory to practice. *Front Neurol*. 2020;11:458. doi:10.3389/fneur.2020.00458
30. Albert MS, DeKosky ST, Dickson D, et al. The diagnosis of mild cognitive impairment due to Alzheimer's disease: recommendations from the National Institute on Aging-Alzheimer's Association workgroups on diagnostic guidelines for Alzheimer's disease. *Alzheimers Dement*. 2011;7:270-279. doi:10.1016/j.jalz.2011.03.008
31. Rensink RA. Change detection. *Annu Rev Psychol*. 2002;53:245-277.
32. Kyllingsbæk S, Bundesen C. Changing change detection: improving the reliability of measures of visual short-term memory capacity. *Psychon Bull Rev*. 2009;16:1000-1010. doi:10.3758/PBR.16.6.1000
33. Cowan N. Metatheory of storage capacity limits. *Behav Brain Sci*. 2001;24:154-176.
34. Yan C-G, Wang X-D, Zuo X-N, Zang Y-F. DPABI: data processing & analysis for (resting-state) brain imaging. *Neuroinformatics*. 2016;14:339-351.
35. Tzourio-Mazoyer N, Landeau B, Papathanassiou D, et al. Automated anatomical labeling of activations in SPM using a macroscopic anatomical parcellation of the MNI MRI single-subject brain. *NeuroImage*. 2002;15:273-289. doi:10.1006/nimg.2001.0978
36. Desikan RS, Ségonne F, Fischl B, et al. An automated labeling system for subdividing the human cerebral cortex on MRI scans into gyral based regions of interest. *NeuroImage*. 2006;31:968-980.
37. Eickhoff SB, Stephan KE, Mohlberg H, et al. A new SPM toolbox for combining probabilistic cytoarchitectonic maps and functional imaging data. *NeuroImage*. 2005;25:1325-1335.
38. Whitfield-Gabrieli S, Nieto-Castanon A. Conn: a functional connectivity toolbox for correlated and anticorrelated brain networks. *Brain Connect*. 2012;2:125-141. doi:10.1089/brain.2012.0073
39. Behzadi Y, Restom K, Liau J, Liu TT. A component based noise correction method (CompCor) for BOLD and perfusion based fMRI. *Neuroimage*. 2007;37:90-101. doi:10.1016/j.neuroimage.2007.04.042
40. Xie L, Wisse LEM, Das SR, et al. Accounting for the confound of meninges in segmenting entorhinal and perirhinal cortices in T1-weighted MRI. *Med Image Comput Comput Assist Interv*. 2016;9901:564-571. doi:10.1007/978-3-319-46723-8_65
41. Yushkevich PA, Pluta JB, Wang H, et al. Automated volumetry and regional thickness analysis of hippocampal subfields and medial temporal cortical structures in mild cognitive impairment. *Hum Brain Mapp*. 2015;36:258-287. doi:10.1002/hbm.22627
42. Van Leemput K, Bakkour A, Benner T, et al. Automated segmentation of hippocampal subfields from ultra-high resolution in vivo MRI. *Hippocampus*. 2009;19:549-557. doi:10.1002/hipo.20615
43. Jenkinson M, Beckmann CF, Behrens TE, Woolrich MW, Smith SM. Fsl. *Neuroimage*. 2012;62:782-790. doi:10.1016/j.neuroimage.2011.09.015
44. Tournier J-D, Smith R, Raffelt D, et al. MRtrix3: a fast, flexible and open software framework for medical image processing and visualisation. *Neuroimage*. 2019;202:116137. doi:10.1016/j.neuroimage.2019.116137
45. Smith RE, Raffelt D, Tournierc J-D, Connelly A. Quantitative streamlines tractography: methods and inter-subject normalisation. *Aperture Neuro*. 2022;1-25.
46. Mccall JD, Vivian Dickens J, Mandal AS, et al. Structural disconnection of the posterior medial frontal cortex reduces speech error monitoring. *Neuroimage Clin*. 2022;33:102934. doi:10.1016/j.nicl.2021.102934
47. Smith RE, Tournier JD, Calamante F, Connelly A. SIFT2: enabling dense quantitative assessment of brain white matter connectiv-

ity using streamlines tractography. *Neuroimage*. 2015;119:338-351. doi:10.1016/j.neuroimage.2015.06.092

48. Baum GL, Cui Z, Roalf DR, et al. Development of structure-function coupling in human brain networks during youth. *Proc Natl Acad Sci U S A*. 2020;117:771-778. doi:10.1073/pnas.1912034117
49. Hotelling H. Relations between two sets of variates. *In Breakthroughs in statistics: methodology and distribution*. 162–190 (New York, NY: Springer New York, 1992).
50. Zhuang X, Yang Z, Cordes D. A technical review of canonical correlation analysis for neuroscience applications. *Hum Brain Mapp*. 2020;41:3807-3833. doi:10.1002/hbm.25090
51. Gonzalez I, Déjean S, Martin P, Baccini A. CCA: an R package to extend canonical correlation analysis. *J Stat Softw*. 2008;23:1-14.
52. Buch AM, Vértes PE, Seidlitz J, Kim SoH, Grosenick L, Liston C. Molecular and network-level mechanisms explaining individual differences in autism spectrum disorder. *Nat Neurosci*. 2023;26:650-663. doi:10.1038/s41593-023-01259-x
53. Zokaei N, Sillence A, Kienast A, et al. Different patterns of short-term memory deficit in Alzheimer's disease, Parkinson's disease and subjective cognitive impairment. *Cortex*. 2020;132:41-50. doi:10.1016/j.cortex.2020.06.016
54. Yeung MK, Chau AK-Y, Chiu JY-C, Shek JT-L, Leung JP-Y, Wong TC-H. Differential and subtype-specific neuroimaging abnormalities in amnestic and nonamnestic mild cognitive impairment: a systematic review and meta-analysis. *Ageing Res Rev*. 2022;80: 101675. doi:10.1016/j.arr.2022.101675
55. Cabeza R, Albert M, Belleville S, et al. Maintenance, reserve and compensation: the cognitive neuroscience of healthy ageing. *Nat Rev Neurosci*. 2018;19:701-710. doi:10.1038/s41583-018-0068-2
56. Gillis MM, Garcia S, Hampstead BM. Working memory contributes to the encoding of object location associations: support for a 3-part model of object location memory. *Behav Brain Res*. 2016;311:192-200. doi:10.1016/j.bbr.2016.05.037
57. Postma A, Kessels R, Vanasselen M. How the brain remembers and forgets where things are: the neurocognition of object-location memory. *Neurosci Biobehav Rev*. 2008;32:1339-1345. doi:10.1016/j.neubiorev.2008.05.001
58. Hales JB, Brewer JB. Parietal and frontal contributions to episodic encoding of location. *Behav Brain Res*. 2013;243:16-20. doi:10.1016/j.bbr.2012.12.048
59. Chechlacz M, Gillebert CR, Vangkilde SA, Petersen A, Humphreys GW. Structural variability within frontoparietal networks and individual differences in attentional functions: an approach using the theory of visual attention. *J Neurosci*. 2015;35:10647-10658. doi:10.1523/JNEUROSCI.0210-15.2015
60. Cai Y, Urgolites Z, Wood J, et al. Distinct neural substrates for visual short-term memory of actions. *Human Brain Mapping*. 2018;39:4119-4133.
61. Garrido MI, Barnes GR, Kumaran D, Maguire EA, Dolan RJ. Ventromedial prefrontal cortex drives hippocampal theta oscillations induced by mismatch computations. *Neuroimage*. 2015;120:362-370. doi:10.1016/j.neuroimage.2015.07.016
62. Johnson EL, Adams JN, Solbakk A-K, et al. Dynamic frontotemporal systems process space and time in working memory. *PLoS Biol*. 2018;16:e2004274. doi:10.1371/journal.pbio.2004274
63. Su M, Hu K, Liu W, et al. Theta oscillations support prefrontal-hippocampal interactions in sequential working memory. *Neurosci Bull*. 2024;40:147-156. doi:10.1007/s12264-023-01134-6
64. Yang Y, Chen Y, Sang F, et al. Successful or pathological cognitive aging? Converging into a "frontal preservation, temporal impairment (FPTI)" hypothesis. *Sci Bull (Beijing)*. 2022;67:2285-2290. doi:10.1016/j.scib.2022.11.004
65. Daume J, Kamiński J, Schjetnan AGP, et al. Control of working memory by phase-amplitude coupling of human hippocampal neurons. *Nature*. 2024;629:393-401. doi:10.1038/s41586-024-07309-z

SUPPORTING INFORMATION

Additional supporting information can be found online in the Supporting Information section at the end of this article.

How to cite this article: Xie Y, Zhao T, Zhang W, et al. Neural deterioration and compensation in visual short-term memory among individuals with amnestic mild cognitive impairment. *Alzheimer's Dement*. 2025;21:e14475. https://doi.org/10.1002/alz.14475